

# Non-phase matched parametric down conversion in an ultrathin nonlinear layer.

C. Okoth<sup>1,2</sup>, A. Cavanna<sup>1,2</sup>, T. Santiago-Cruz<sup>1,2</sup> & M. V. Chekhova<sup>1,2,3</sup>  
(Dated: March 1, 2019)

Spontaneous parametric down-conversion (SPDC) is a well-developed tool to produce entangled photons for various applications in quantum technology such as quantum imaging [1–3], quantum key distribution [4, 5] and quantum metrology [6, 7]. So far, SPDC has exclusively been observed in the phase matched regime: when the emitted daughter photons conserve the momentum of the pump photon. Phase matching is often challenging to satisfy; not only does it restrict the choice of non-linear materials to work with but it also greatly limits the angular and frequency spectral width of SPDC. Reducing the non-linear interaction length to microscopic scales or lower, relaxes the phase matching condition to the point where two-photon radiation can be emitted into a huge range of angles, across a massive bandwidth whilst still maintaining the quantum correlations that make SPDC such an important tool. Despite the active search, SPDC is yet to be observed from ultrathin or monoatomic layers [8–10]. Here we demonstrate efficient generation of SPDC in a strongly nonlinear layer with a thickness equal to a few coherence lengths. Using a 6.8  $\mu\text{m}$  layer of lithium niobate pumped with a moderate-power CW laser we register photon pairs generated via SPDC. The two-photon radiation displays both an extremely broad frequency spectrum and a huge degree of entanglement. Whilst the non-phase matched pair emission from lithium niobate has record breaking spatio-temporal correlation widths and large quantum information capacity, we expect that similar sources can be realized on thinner platforms, not only compounding the aforementioned effects, but also allowing easy integrability on optical chips.

For SPDC, the probability that a pump photon with wavevector  $\vec{k}_p$  decays into two daughter photons, signal and idler with wavevectors  $\vec{k}_{s,i}$ , strongly depends on the wavevector mismatch  $\Delta\vec{k} \equiv \vec{k}_s + \vec{k}_i - \vec{k}_p$ . In a material of length  $L$  with the nonlinear susceptibility  $d$ , this probability is

$$P \propto d^2 L^2 F_{pm}(\Delta k_{\parallel}) F_p(\Delta k_{\perp}), \quad (1)$$

where  $F_{pm}$  is the phase matching function,

$$F_{pm}(\Delta k_{\parallel}) = \text{sinc}^2\left(\frac{\Delta k_{\parallel} L}{2}\right), \quad (2)$$

and  $F_p$  the pump function,

$$F_p(\Delta k_{\perp}) = e^{-(\Delta k_{\perp} w)^2}. \quad (3)$$

The phase matching function depends on the parallel component of the wavevector mismatch,  $\Delta k_{\parallel}$ , whilst the pump function, assuming a Gaussian beam profile with waist  $w$ , centered on the non-linear material, depends on the perpendicular wavevector component,  $\Delta k_{\perp}$ .

In a phase-matched process,  $\Delta k_{\parallel} = 0$ : the longitudinal momentum of the pump photon is conserved by the daughter photons. This leads to a quadratic increase in efficiency with the length of the non-linear material as newly generated daughter photons constructively interfere with daughter photons generated near the start of the non-linear material. However, this is a special case and is satisfied only in a few non-linear materials with the appropriate electronic and optical properties. More generally  $\Delta k_{\parallel} \neq 0$ , however if the length of the non-linear material is less than  $L_c = \frac{\pi}{\Delta k_{\parallel}}$ , referred to as the coherence length [11], then, regardless of the physical properties of the non-linear material, the probability  $P$  of SPDC is non-zero. Simply put, this is because the generation of daughter photons cannot move out of phase over the short non-linear interaction length set by  $L_c$ . According to Eqs. (1,2),  $P$  oscillates with the length  $L$ , where the peaks occur at odd multiples of the coherence length.

Whilst the possible emission angles and frequencies for the signal and idler photons are usually determined by the phase matching function (2), the angular and frequency *correlation* widths are determined by the pump function in (3), and will be small if the pump has a large beam waist. For this reason, SPDC from an ultra-thin layer should produce photon pairs that are highly entangled in angle and frequency: while these parameters are very uncertain for a single photon, they are known with certainty when the conjugate photon is detected.

Fig. 1 a shows the allowed wavevector mismatch for a thick crystal and an ultra-thin layer. Whilst the thick crystal restricts the signal and idler angles and frequencies, the ultra-thin layer allows a broad range of modes to be populated. The calculated frequency - angular spectrum for SPDC from a single coherence length or its odd multiple (Fig. 1 c,d) is far broader than any SPDC spectra observed from a macroscopically thick crystal (Fig. 1 b).

The reduced interaction length, however, leads to a lower SPDC efficiency. This can be partly compensated for by using a highly nonlinear medium. Here we use an x-cut lithium niobate (LN) crystal and, by taking

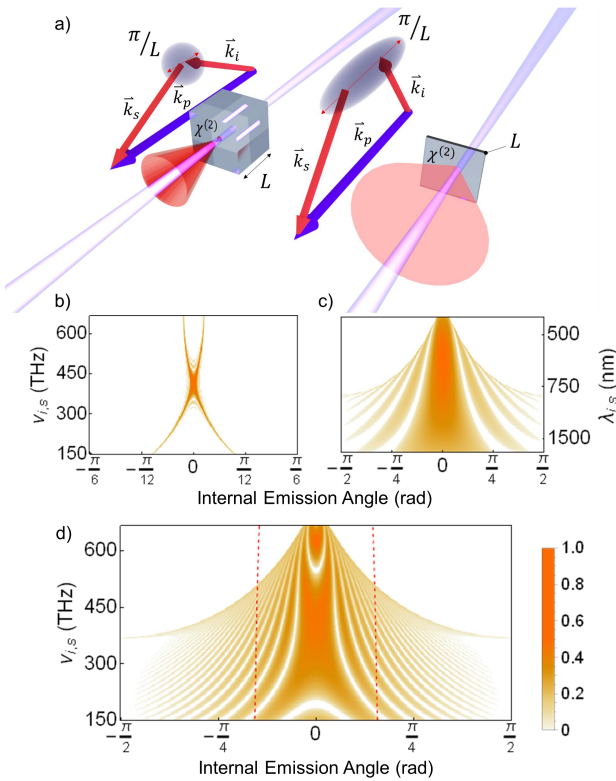


FIG. 1. (a) Comparison of the SPDC emission in a thick (left) and ultrathin (right) nonlinear layer orthogonal to the pump. In the second case, the allowed wavevector mismatch along the pump direction is very large, which results in a broad spectrum, both in frequency and angle. As an example, the middle panels show the frequency-angular spectrum calculated for a phase matched type-I BBO crystal with  $L = 1$  mm (b) and non-phase matched type-0 lithium niobate crystal with  $L = L_c = 1.3 \mu\text{m}$  (c). The pump wavelength is 405 nm and beam waist 100  $\mu\text{m}$ . Note the different x-axis scales between (b) and (c). The bottom panel (d) is the frequency-angular spectrum expected for a non-phase matched type-0 lithium niobate crystal with  $L = 5L_c$ . The red dashed lines show the angle of internal reflection, which limits the angle collected.

advantage of the fact that we no longer need to phase match, utilize the large  $d_{33}$  component of the nonlinear susceptibility tensor by correctly orienting the pump polarization. The  $d_{33}$  component of LN (40 pm/V) is roughly 40 times stronger than the effective susceptibility of  $\beta$ -Barium borate (BBO), a standard crystal used for SPDC experiments [11].

The experimental setup is shown in Fig. 2. The sample tested was a thin layer of magnesium doped LN grown on a 500  $\mu\text{m}$  fused silica layer. The  $z$ -axis of LN was in the plane of the layer. The thickness of the sample varied from 5.9  $\mu\text{m}$  to 6.8  $\mu\text{m}$ , due to the non-uniform fabrication of the wafer. Therefore by scanning the LN in the  $z$ -y plane it was possible to tune the length.

Despite the use of the highest non-linear component available in LN, the efficiency remained several orders of

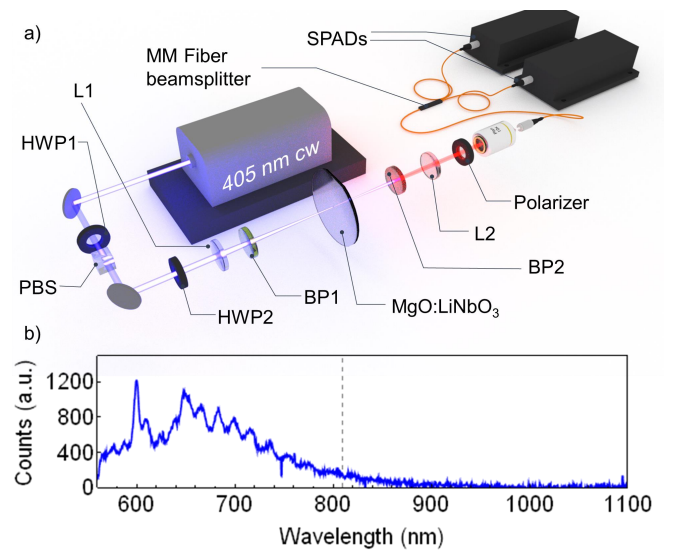


FIG. 2. The setup used to detect SPDC emission from lithium niobate (a) and the fluorescence spectrum measured with a spectrometer (b). The dashed line indicates the degenerate wavelength where most of the measurements were taken.

magnitude lower than for phase-matched SPDC. As a result, fluorescence, which can usually be disregarded when working with phase matched SPDC, became the dominant process in the spectral region that we were interested in. The measured fluorescence (Fig. 2 b) was more than an order of magnitude stronger than the expected SPDC emission. Due to the broadband nature of non-phase matched SPDC, distinguishing the two-photon radiation from fluorescence could only be done using correlation measurements.

The correlation measurements were performed using Hanbury Brown - Twiss (HBT) setup (Fig. 2a). To begin with, the normalized second-order correlation function  $g^{(2)}(\tau)$  was measured, shown in Fig. 3 a. Strong two-photon correlations were observed, as we see from the peak at zero delay. Further, the value of  $g^{(2)}(0)$  was measured as a function of the single photon rate in each detector. This was varied by changing the pump power (see Fig. 3 b). The measured value of  $g^{(2)}(0) - 1$  follows an inverse dependence on the mean photon number, as expected [12] for photon pair generation. High values of  $g^{(2)}(0)$ , also known in the literature as coincidences-to-accidentals ratio (CAR), and its inverse dependence with the mean number of photons is convincing evidence of two-photon light generation.

The measured polarization dependence of the coincidence count rate (Fig. 3 c) confirm that the SPDC is due to the  $d_{33}$  component of the nonlinear susceptibility tensor, with the pump, signal, and idler photons polarized along  $z$ . Indeed, the SPDC was noticeable only when the signal and idler photons were polarized along the  $z$

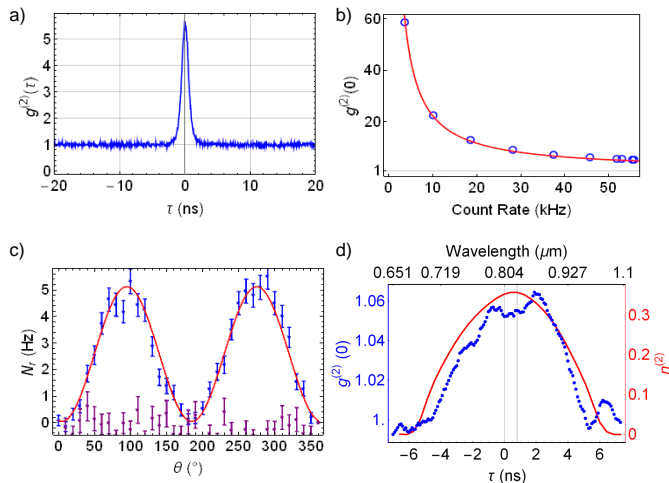


FIG. 3. Correlation measurements performed to characterise the SPDC emission from the LN sample. (a) The normalised two-photon temporal correlation function. (b) The normalised correlation function at zero time delay measured versus the total number of detected photons (blue points) and fitted with an inverse dependence, which is indicative of two-photon radiation (red line). (c) The rate of real coincidences versus the pump polarisation direction, for the emission polarised along  $z$  (blue points, red fit) and along  $y$  (purple points). (d) The normalized temporal correlation function measured after propagation through a dispersive fiber. The temporal delay is mapped into units of wavelength. The double photon quantum efficiency (see Methods) is shown in red.

axis, in this case the coincidence rate depended on the angle  $\theta$  between the pump polarization and the  $y$  axis as  $\sin^2(\theta)$  (blue points, red fit). For the emission polarized along the  $y$ -axis, no real coincidences were observed (purple points).

The SPDC spectrum was measured using single-photon spectroscopy (SPS) [13, 14] (see Methods), which allowed us to distinguish it from the fluorescence spectrum. Light generated from LN was coupled into a dispersive fiber. After propagation through the fiber the two-photon wavepackets spread in time, and the delay time between the signal and idler photons was mapped to a frequency difference. The measured normalized correlation function after the propagation through 160 m of optical fibre is shown in Fig. 3 d. The width of the peak corresponds to 200 nm, which is less than the expected width of 600 nm (see Fig. 1 d) because of the relatively narrow sensitivity range of the single-photon detectors (see Methods) and frequency-dependent fiber coupling. The biphoton correlation time, given by the inverse spectral width [13], is then estimated to be 10 fs. Without the narrowing of the spectrum caused by the detector sensitivity, the correlation time would be as short as 3 fs.

To demonstrate the high degree of frequency entanglement, we measured the joint spectral intensity (JSI),

quantifying the joint probability  $P(\omega_s, \omega_i)$  of the signal and idler photons having frequencies  $\omega_s, \omega_i$ , respectively. The JSI was reconstructed using stimulated emission tomography (SET, see Fig. 4a and Methods). The use of SET significantly amplified the emission, allowing us to characterize the JSI by measuring the spectrum of a single bright beam as opposed to the registration of coincidences. By pumping with the second harmonic of the Nd:YAG laser at 532 nm and tuning the seed beam wavelength between 1500 and 1620 nm, a small part of the JSI (Fig. 4b,c) was mapped out as shown in Fig. 4 d. Because of the narrow tuning range of the seed, the full spectral range of SPDC could not be obtained. Still, the SET results demonstrate tight frequency correlations (0.6 THz), within a 13 THz range of the JSI, which confirms a degree of entanglement of at least 20, a value that could be far higher when taking into account the broad spectral width.

Generating entangled photons with broad spectral and angular width has been a long standing goal in the field of quantum optics [15–17]. Highly non-linear ultrathin and monoatomic layers not only provide a platform on which to achieve this goal but also promise spatio-temporal correlations tighter than anything currently observed. The ultrashort correlation time associated with a broad frequency spectrum can be used to synchronize distant clocks [7]. Meanwhile, tight spatial correlations can be used to dramatically improve the resolution of many quantum imaging techniques such as ghost imaging and imaging with undetected photons [1–3, 18]. In addition, both the angle of emission and frequency can be used as variables for encoding quantum information [19, 20]: the high degree of entanglement of photon pairs from non-phaseshifted SPDC offers them an unprecedentedly high information capacity.

## METHODS

*Scanning the sample thickness.* The non-phase matched SPDC emission has an oscillatory dependence on the layer thickness, being maximum for odd multiples of  $L_c$  and zero for even multiples of  $L_c$ . In the case of 405 nm pump and degenerate SPDC at 810 nm the coherence length for LN is  $L_c = 1.37 \mu\text{m}$ . By varying the position of the pump beam on the sample, we could scan its thickness (see Supplementary Information, Fig. 5). The maximal emission happens in the thicker region of the sample, which corresponds to about  $5L_c$ , as shown in Fig. 6 of the Supplementary material. Note that the rate of SPDC for thickness  $L_c$  would be the same as for thickness  $5L_c$ , but only a thicker sample was available for us for technical reasons.

*Registration of coincidences.* Two-photon coincidences were detected using a Hanbury Brown-Twiss setup (Fig. 2a). The CW pump beam was centered at 405 nm

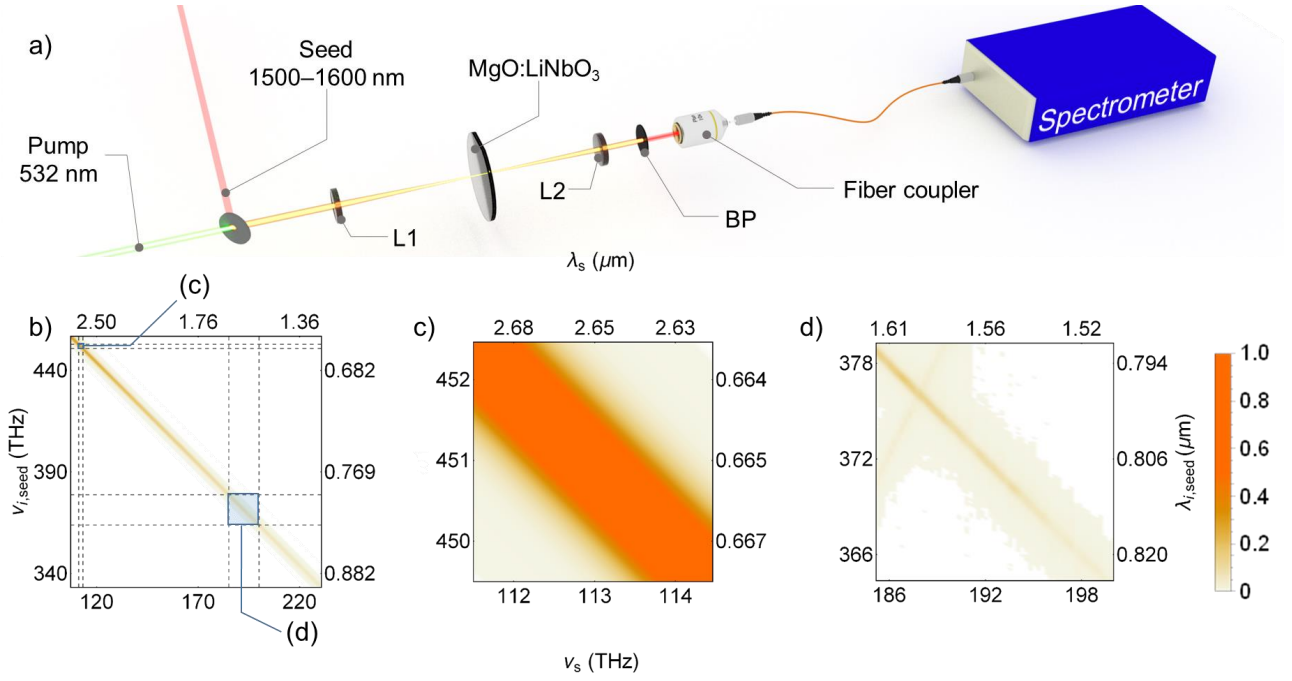


FIG. 4. The setup for the SET measurement (a) and the calculated JSI for  $5.8 \mu\text{m}$  LN pumped at  $532 \text{ nm}$  (b), with a zoomed in interval (c) to emphasise the small width. L1,2 are lenses and BP is a band-pass filter blocking the pump and the seed. Panel d shows a fragment of JSI measured using SET, with the bounds limited by the tunability of the seed. The fainter line with a positive tilt in (d) is due to second harmonic generation of the seed.

and had a maximum power output of  $60 \text{ mW}$ . The pump polarization and power were controlled using a polarizing beam splitter (PBS) and two half wave plates (HWP). The pump was focused, using a  $100 \text{ mm}$  lens (L1), into the LN sample, which was placed on a translation stage to provide movement in the  $z$ - $y$  plane of the crystal structure (see Supplementary material). To avoid additional sources of fluorescence the pump was filtered using a  $405 \text{ nm}$  bandpass (BP1) immediately after the L1. The resulting emission was filtered of the pump, collected using a  $100 \text{ mm}$  lens (L2) and coupled into a multimode fiber beam splitter. To isolate the breakdown flash effect of the single-photon detectors in time [21], two  $20 \text{ m}$  long fibers were placed after the fiber beam splitter. The photons were registered on two Perkin-Elmer visible-range single photon counting modules. The arrival time of each photon was recorded using a Swabian Instruments Time Tagger. To find the real coincidence rate, the accidental coincidence rate was subtracted,

$$N_r = N_c - N_1 N_2 T_c, \quad (4)$$

where  $N_c$  is the total coincidence rate,  $N_{1,2}$  are the single photon count rates into detector 1 and 2 respectively, and  $T_c$  is the coincidence resolution time. The normalized second-order correlation function, or equivalently the CAR, was calculated using

$$g^{(2)} = \frac{N_c}{N_1 N_2 T_c}. \quad (5)$$

*Single-photon spectroscopy.* To measure the SPDC spectrum, we introduced a  $160 \text{ m}$  SMF28 fibre to the set up shown in Fig. 2a, between the LN output and the MM fiber beam splitter. In addition, L1 was replaced with a  $20 \text{ mm}$  lens to decrease the pump beam waist in an effort to lower the number of spatial modes and increase the coupling efficiency into the SMF28 fiber. The dispersive temporal walk-off in the fibre was used to split the frequency modes temporally and led to a difference in photon arrival times corresponding to a specific frequency difference. To calibrate the arrival time differences, the radiation in one arm of the fiber beam splitter was sent through a  $10 \text{ nm}$  broad interference filter centered at the calibration wavelength. The emission was recoupled into the  $20 \text{ m}$  MM fibre after passing through the filter and the coincidences between the first and the second detector were measured as a function of the difference in photon arrival times. This was done for six interference filters and a calibration curve between time differences and frequency differences was fitted with a cubic polynomial (see Fig. 7 of the Supplementary material). As this type of measurement was based on collecting correlated photons, any frequency dependent loss on one photon was mirrored on its conjugate. This affected the spectral sensitivity of the detectors which, accounting for the mirrored loss in the visible region, is shown as the red curve in Fig. 3 d.

*Stimulated emission tomography.* A custom optical

parametric amplifier (OPA) was built using a pair of bismuth triborate (BiBO) crystals (see Fig. 8 of the Supplementary material) with type-I phase matching. It was pumped by a frequency doubled Nd:YAG laser (532 nm) with a 20 ps pulse width and 1 kHz repetition rate and amplified a CW source tunable between 1500 nm and 1620 nm. The output radiation of the OPA had the same pulse properties as the pump beam and was used as a seed for LN in the SET measurement. To compensate for any temporal walk-off between the pump and the seed a delay line between the two beams was built. A PBS and HWP were added to both arms to control both the power and the polarization of the seed and the pump locally. The idler beam of the OPA was suppressed by the PBS in the pump arm and a frequency filter in the seed arm. The seed and pump beams were overlapped spatially and temporally (see Fig. 4 a) and focused into the LN sample using a 400 mm lens (L1). The seed wavelength was scanned from 1500 nm to 1620 nm and the stimulated PDC radiation was registered with an Avantes visible-range spectrometer. The resulting spectra were plotted for each seed frequency probed to reconstruct the JSI.

The expected JSI for collinear SPDC is

$$P(\omega_s, \omega_i) \propto F_{pm}(\omega_s, \omega_i) F_p^{(\omega)}(\omega_s, \omega_i), \quad (6)$$

where  $F_{pm}(\omega_s, \omega_i)$  is given by (2) with  $\Delta k_{\parallel} = \Delta k_{\parallel}(\omega_s, \omega_i)$  and, for a Gaussian pump,

$$F_p^{(\omega)}(\omega_s, \omega_i) = e^{-\frac{1}{2} \left( \frac{\omega_s + \omega_i - \omega_{p0}}{\sigma} \right)^2}, \quad (7)$$

$\omega_{p0}$  is the central pump frequency and  $\sigma$  is the pump spectral width [22].

*The degree of entanglement.* To estimate the degree of entanglement we use the measure introduced by Fedorov [23]. It is defined as the ratio  $R = \Delta/\delta$ , where  $\Delta$  is the unconditional width of the JSI, i.e., the spectral width of the signal (idler) radiation, and  $\delta$  is the corresponding conditional (correlation) width. If the amplitude of JSI has no strongly frequency-dependent phase, the Fedorov ratio  $R$  is approximately equal to the Schmidt number  $K$  [24, 25]. Otherwise,  $R$  only characterizes part of the entanglement and in some cases [26] underestimates it. In Fig. 4 c,  $\delta$  is the width of the JSI cross-section, 0.6 THz. As to  $\Delta$ , it was measured to be 13 THz but it is limited by the range probed in experiment. Therefore, we can confirm  $R \geq 20$  but the degree of entanglement should be at least an order of magnitude larger, according to Fig. 4 b.

### Acknowledgements

We acknowledge the financial support by Deutsche Forschungsgemeinschaft (DFG) (CH-1591/3-1, JO-1090/3-1).

- [1] G. B. Lemos, V. Borish, G. D. Cole, S. Ramelow, R. Lapkiewicz, and A. Zeilinger, "Quantum imaging with undetected photons," *Nature*, vol. 512, no. 7515, p. 409, 2014.
- [2] T. Pittman, Y. Shih, D. Strekalov, and A. Sergienko, "Optical imaging by means of two-photon quantum entanglement," *Physical Review A*, vol. 52, no. 5, p. R3429, 1995.
- [3] G. Brida, M. Genovese, and I. R. Berchera, "Experimental realization of sub-shot-noise quantum imaging," *Nature Photonics*, vol. 4, no. 4, p. 227, 2010.
- [4] Y. Adachi, T. Yamamoto, M. Koashi, and N. Imoto, "Simple and efficient quantum key distribution with parametric down-conversion," *Physical review letters*, vol. 99, no. 18, p. 180503, 2007.
- [5] T. Jennewein, C. Simon, G. Weihs, H. Weinfurter, and A. Zeilinger, "Quantum cryptography with entangled photons," *Physical Review Letters*, vol. 84, no. 20, p. 4729, 2000.
- [6] L.-A. Wu, H. Kimble, J. Hall, and H. Wu, "Generation of squeezed states by parametric down conversion," *Physical review letters*, vol. 57, no. 20, p. 2520, 1986.
- [7] A. Valencia, G. Scarcelli, and Y. Shih, "Distant clock synchronization using entangled photon pairs," *Applied Physics Letters*, vol. 85, no. 13, pp. 2655–2657, 2004.
- [8] H. D. Saleh, S. Vezzoli, L. Caspani, A. Branny, S. Kumar, B. D. Gerardot, and D. Faccio, "Towards spontaneous parametric down conversion from monolayer mos 2," *Scientific reports*, vol. 8, no. 1, p. 3862, 2018.
- [9] M. Tokman, Z. Long, S. AlMutairi, Y. Wang, V. Vdovin, M. Belkin, and A. Belyanin, "Purcell enhancement of the parametric down-conversion in two-dimensional nonlinear materials," *APL Photonics*, vol. 4, no. 3, p. 034403, 2018.
- [10] S. Yamashita, "Nonlinear optics in carbon nanotube, graphene, and related 2d materials," *APL Photonics*, vol. 4, no. 3, p. 034301, 2018.
- [11] R. W. Boyd, *Nonlinear optics*. Elsevier, 2003.
- [12] O. A. Ivanova, T. S. Iskhakov, A. N. Penin, and M. V. Chekhova, "Multiphoton correlations in parametric down-conversion and their measurement in the pulsed regime," *Quantum Electronics*, vol. 36, no. 10, p. 951, 2006.
- [13] A. Valencia, M. V. Chekhova, A. Trifonov, and Y. Shih, "Entangled two-photon wave packet in a dispersive medium," *Physical review letters*, vol. 88, no. 18, p. 183601, 2002.
- [14] M. Avenhaus, A. Eckstein, P. J. Mosley, and C. Silberhorn, "Fiber-assisted single-photon spectrograph," *Optics letters*, vol. 34, no. 18, pp. 2873–2875, 2009.
- [15] M. B. Nasr, S. Carrasco, B. E. Saleh, A. V. Sergienko, M. C. Teich, J. P. Torres, L. Torner, D. S. Hum, and M. M. Fejer, "Ultrabroadband biphotons generated via chirped quasi-phase-matched optical parametric down-conversion," *Physical review letters*, vol. 100, no. 18, p. 183601, 2008.
- [16] C. Bernhard, B. Bessire, T. Feurer, and A. Stefanov, "Shaping frequency-entangled qudits," *Physical Review A*, vol. 88, no. 3, p. 032322, 2013.
- [17] K. Katamadze, N. Borshechkaya, I. Dyakonov, A. Paterova, and S. Kulik, "Broadband biphotons in a single spatial mode," *Physical Review A*, vol. 92, no. 2,

- p. 023812, 2015.
- [18] M. D'Angelo, A. Valencia, M. H. Rubin, and Y. Shih, "Resolution of quantum and classical ghost imaging," *Physical Review A*, vol. 72, no. 1, p. 013810, 2005.
- [19] L. Oslslager, J. Cussey, A. T. Nguyen, P. Emplit, S. Massar, J.-M. Merolla, and K. P. Huy, "Frequency-bin entangled photons," *Physical Review A*, vol. 82, no. 1, p. 013804, 2010.
- [20] J. Rarity and P. Tapster, "Experimental violation of bells inequality based on phase and momentum," *Physical Review Letters*, vol. 64, no. 21, p. 2495, 1990.
- [21] R. Newman, "Visible light from a silicon p- n junction," *Physical review*, vol. 100, no. 2, p. 700, 1955.
- [22] M. Hendrych, M. Micuda, and J. Torres, "Tunable control of the frequency correlations of entangled photons," *Optics letters*, vol. 32, no. 16, pp. 2339–2341, 2007.
- [23] M. Fedorov, M. Efremov, A. Kazakov, K. Chan, C. Law, and J. Eberly, "Packet narrowing and quantum entanglement in photoionization and photodissociation," *Physical Review A*, vol. 69, no. 5, p. 052117, 2004.
- [24] Y. M. Mikhailova, P. A. Volkov, and M. V. Fedorov, "Biphoton wave packets in parametric down-conversion: Spectral and temporal structure and degree of entanglement," *Physical Review A*, vol. 78, p. 062327, 2008.
- [25] G. Brida, V. Caricato, M. V. Fedorov, M. Genovese, M. Gramegna, and S. P. Kulik, "Characterization of spectral entanglement of spontaneous parametric-down conversion biphotons in femtosecond pulsed regime," *EPL*, vol. 87, p. 64003, 2009.
- [26] F. Just, A. Cavanna, M. V. Chekhova, and G. Leuchs, "Transverse entanglement of biphotons," *New Journal of Physics*, vol. 15, no. 8, p. 083015, 2013.

## SUPPLEMENTARY INFORMATION

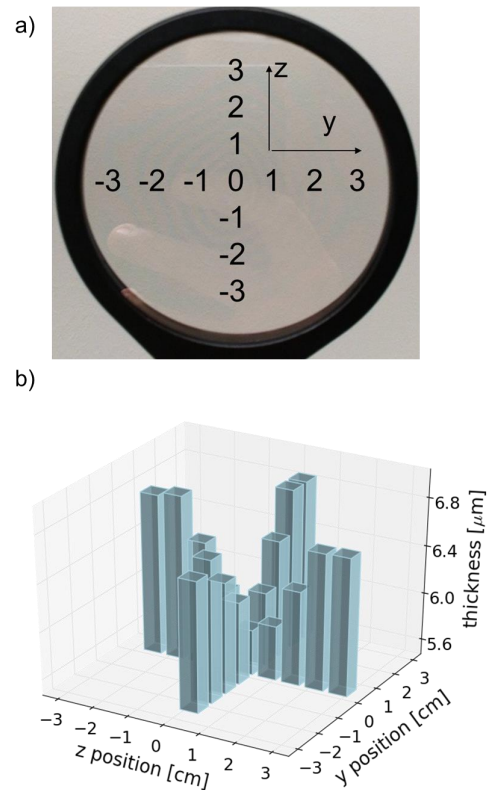


FIG. 5. The thickness of the LN wafer. (a) An image of the sample with numbered points where the sample thickness was measured. (b) The sample thickness for each measured point, the sample varies from roughly  $4L_c$ , at the center, to about  $5L_c$  at the edge.

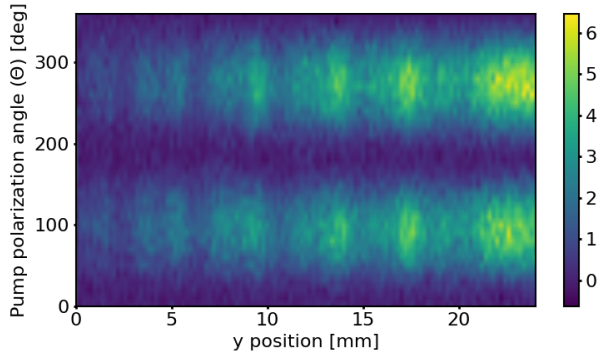


FIG. 6. Coincidence rate for z-polarized emission as a function of the y position and the pump polarization. At position '0' the crystal thickness corresponds to about  $4L_c$  and therefore no SPDC is expected. On the contrary, at the edge of the crystal its thickness is about  $5L_c$  and therefore we expect the maximum emission as confirmed by the increased coincidence rate. Coincidences and therefore SPDC are present only when the pump is polarized along the z axis (which corresponds to 90 and 270 degrees when the polarisation angle is measured from the y axis).

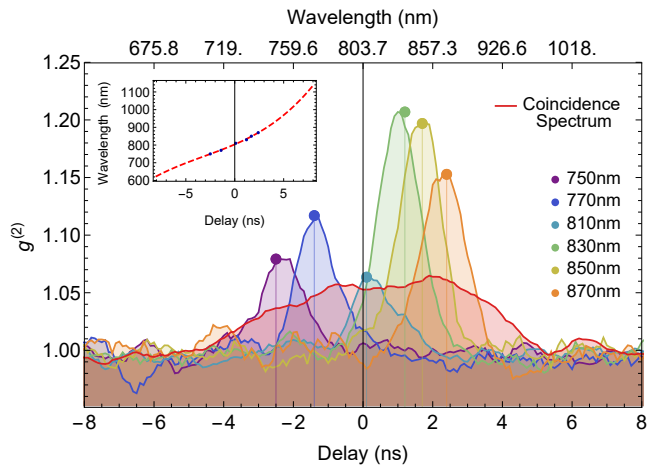


FIG. 7. The normalised correlation function for different time delays for the SPS measurement. Each narrow peak corresponds to a calibration wavelength and the total coincidence spectrum, broadened due to the propagation through the fiber, is shown in red. The inset shows the calibration curve to map time differences to wavelength differences. The experimentally found blue points are fitted with a cubic polynomial in red.

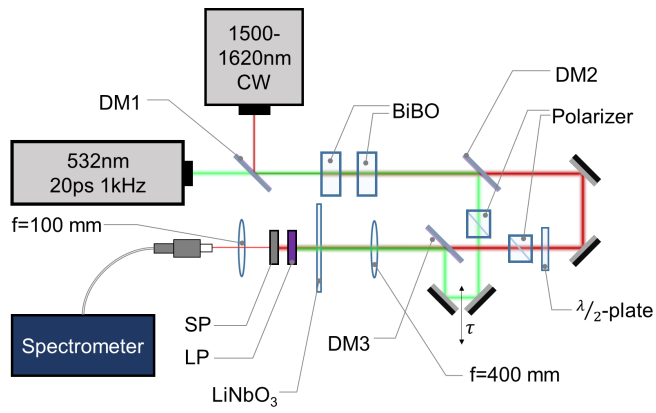


FIG. 8. A schematic of the setup used to reconstruct the JSI using SET. DM1,2 and 3 denote dichroic mirrors that split 532nm and IR wavelengths. SP and LP denote short and long pass filters to remove the pump and seed wavelengths.  $\tau$  is the delay line that compensates for the temporal walk-off between the pump and seed beams.